

# We are IntechOpen, the world's leading publisher of Open Access books Built by scientists, for scientists

6,900

Open access books available

186,000

International authors and editors

200M

Downloads

Our authors are among the

154

Countries delivered to

TOP 1%

most cited scientists

12.2%

Contributors from top 500 universities



WEB OF SCIENCE™

Selection of our books indexed in the Book Citation Index  
in Web of Science™ Core Collection (BKCI)

Interested in publishing with us?  
Contact [book.department@intechopen.com](mailto:book.department@intechopen.com)

Numbers displayed above are based on latest data collected.  
For more information visit [www.intechopen.com](http://www.intechopen.com)



# Fractal Analysis of Micro Self-Sharpening Phenomenon in Grinding with Cubic Boron Nitride (cBN) Wheels

Yoshio Ichida  
 Utsunomiya University,  
 Japan

## 1. Introduction

Self-sharpening phenomenon of the grain cutting edges during grinding is the main factor controlling the performance and the tool life of grinding wheels. Therefore, many studies on the relationship between the wear behavior and the self-sharpening of the grain cutting edges have been carried out (Yoshikawa, 1960; Tsuwa, 1961; Ichida et al., 1989, 1995; Malkin, 1989; Show, 1996). However, it is very difficult to evaluate this relation quantitatively because of the complexity in wear mechanism and the irregularity in shape and distribution of the grain cutting edges (Webster & Tricard, 2004). Especially, self-sharpening of the cutting edges in the grinding process with cBN wheels has not yet been clarified sufficiently (Ichida et al. 1997, 2006; Guo et al., 2007). To develop an innovative machining system using cBN grinding wheels, it is essential to clarify the self-sharpening mechanism due to the micro fracturing of the cutting edges that is the most important factor controlling the grinding ability of cBN wheel during the grinding process (Ichida et al. 2006; Kalpakjian, 1995; Comley et al., 2006).

The main purpose of this study is to evaluate quantitatively such a complicated self-sharpening phenomenon of the cutting edges in cBN grinding on the basis of fractal analysis. The changes in three-dimensional surface profile of cBN grain cutting edge in the grinding process are measured using a scanning electron microscope with four electron detectors and evaluated by means of fractal dimension.

## 2. Three-dimensional fractal analysis

There are several methods for calculating fractal dimension (Mandelbrot, 1983; Mandelbrot et al. 1984; Hagiwara et al., 1995; Itoh et al., 1990). In this report, we have used a 3D-fractal analysis that is expanded based on the idea in the fractal analysis using two-dimensional mesh counting method (Sakai et al., 1998). The analysis method is shown as follows. A 3D-profile under test is divided by cube grid with a mesh size of  $r$ . And then, the number of cubes intersected with 3D-profile  $N(r)$  is counted. If there is a fractal nature in this 3D-profile, the relationship between  $N(r)$ ,  $r$  and fractal dimension  $D_s$  is given by

$$N(r) = \alpha \cdot r^{-D_s} \quad (1)$$

where  $\alpha$  is constant number.

Area of square with mesh size  $r$  is expressed  $r^2$ . Therefore, the surface area of 3D-profile  $S(r)$  based on  $N(r)$  is given by

$$S(r) = r^2 \cdot N(r) = \alpha \cdot r^2 \cdot r^{-D_s} \quad (2)$$

If the logarithm of both sides is taken, eq. (2) is rewritten as follows;

$$\log S(r) = \log \alpha + (2 - D_s) \log r \quad (3)$$

Fractal dimension  $D_s$  is calculated by the following equation using the proportionality constant between  $\log S(r)$  and  $\log r$  in eq. (3).

$$D_s = 2 - \frac{d \log S(r)}{d \log r} \quad (4)$$

However, actual fractal analysis is conducted according to the following procedures by computer processing in this study. As shown in Fig. 1 (a), a square grid with mesh size  $r_1$  is set on a 3D-profile of the top surface of grain cutting edge. It is divided to two triangular elements with mesh size  $r_1$ . Surface areas of each triangle  $s_1(r_1)$  and  $s_2(r_1)$  are evaluated using height coordinates in each grid point and  $S(r_1)$  is decided by sum of these surface areas. Next, as shown in Fig. 1 (b), each triangle is divided with mesh size  $r_2$  that is half a size of  $r_1$ . Surface areas of 8 triangles  $s_1(r_2), \dots, s_8(r_2)$  are evaluated using height coordinates in 9 grid points and  $S(r_2)$  is decided by sum of these surface areas. In addition, as shown in Fig. 1 (c), 8 triangles are divided with mesh size  $r_3$  that is half a size of  $r_2$ . Surface areas of 32 triangles  $s_1(r_3), \dots, s_{32}(r_3)$  are evaluated using height coordinates in 25 grid points and  $S(r_3)$  is decided by sum of these surface areas. Afterward, mesh size  $r$  is scaled down and the surface area of 3D-profile is evaluated as follows;

$$S(r_n) = \sum_{i=1}^{2^{2n-1}} s_i(r_n) \quad (5)$$

On the basis of these equations,  $r$  is taken on the horizontal log axis, and  $S(r)$  is taken on the vertical log axis. When data points are on a straight line in double log plot, fractal dimension  $D_s$  is given by a slope of the straight line. Figure 2 shows an example of relationship between  $S(r)$  and  $r$  (Sample: surface profile of cBN cutting edge shown in Fig.1). Fractal nature is approved in a region of  $0.4 < r < 4 \mu\text{m}$ . From a slope of the straight line, it is decided that fractal dimension is 2.015.

### 3. Three-dimensional observation of wheel working surface

#### 3.1 Experimental procedure

Grinding experiments were conducted with surface plunge grinding method on a horizontal spindle surface grinding machine. The schematic illustration of the experimental setup is shown in Fig. 3. A vitrified cBN wheel with a replaceable cBN segment shown in Fig. 3 was used to observe directly the profile of the wheel surface in the grinding process using a three-dimensional (3D) scanning electron microscope with four electron probes (3D-SEM/

EDM3000) (Ichida, 2008). The cBN segment detached for the observation can be precisely returned to former state again. It was confirmed experimentally that the cBN wheel with the replaceable cBN segment has almost the same grinding ability as the usual complete cBN wheel (Fujimoto, 2006).

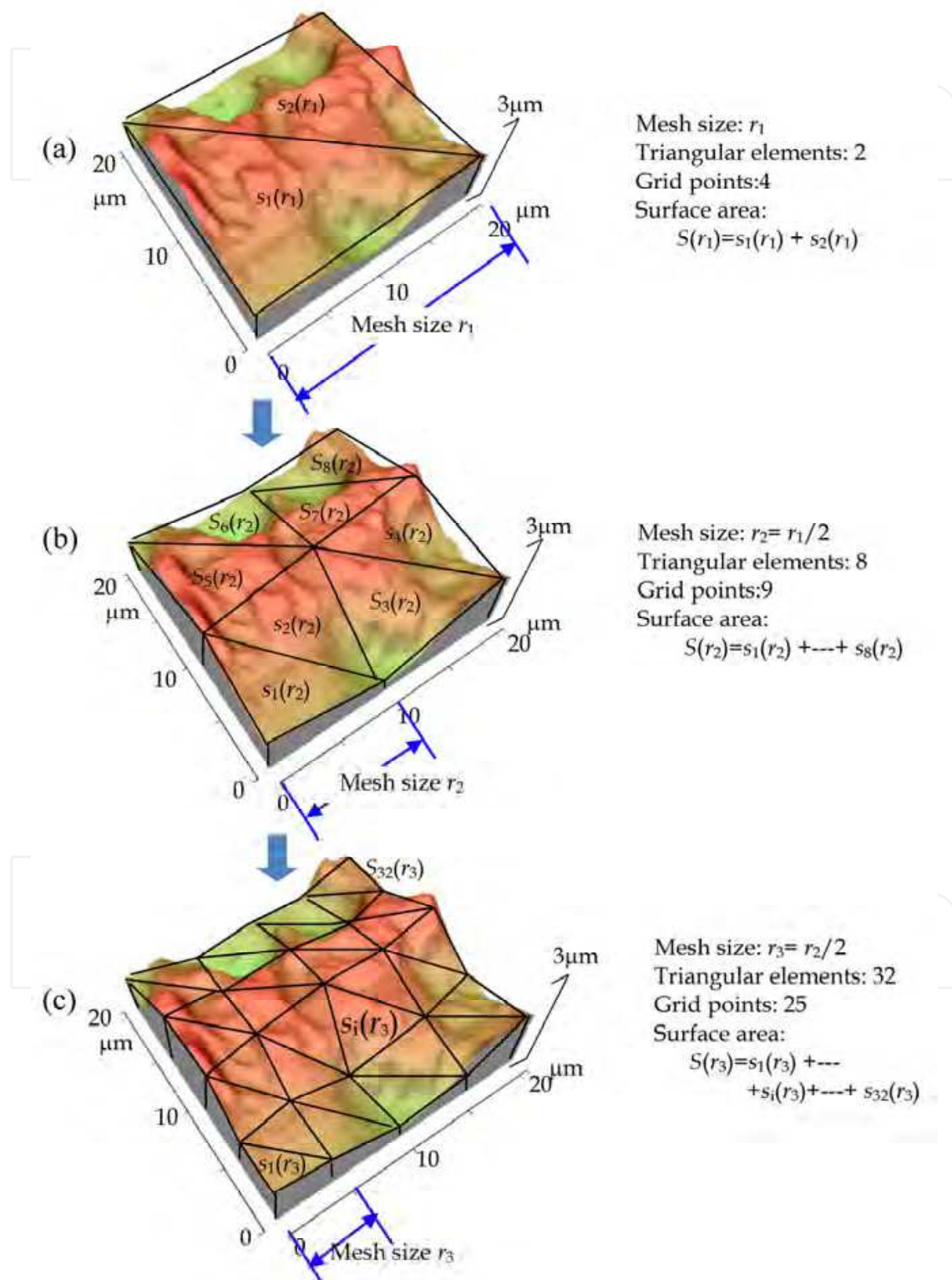


Fig. 1. Method of 3D-fractal analysis (Sample: surface profile of cBN abrasive grain).

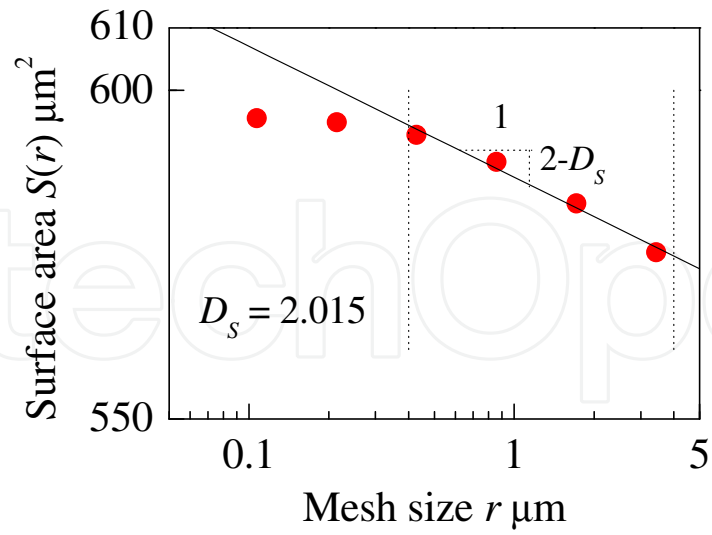


Fig. 2. Relationship between surface area  $S(r)$  and mesh size  $r$  (Sample: surface profile shown in Fig.1).

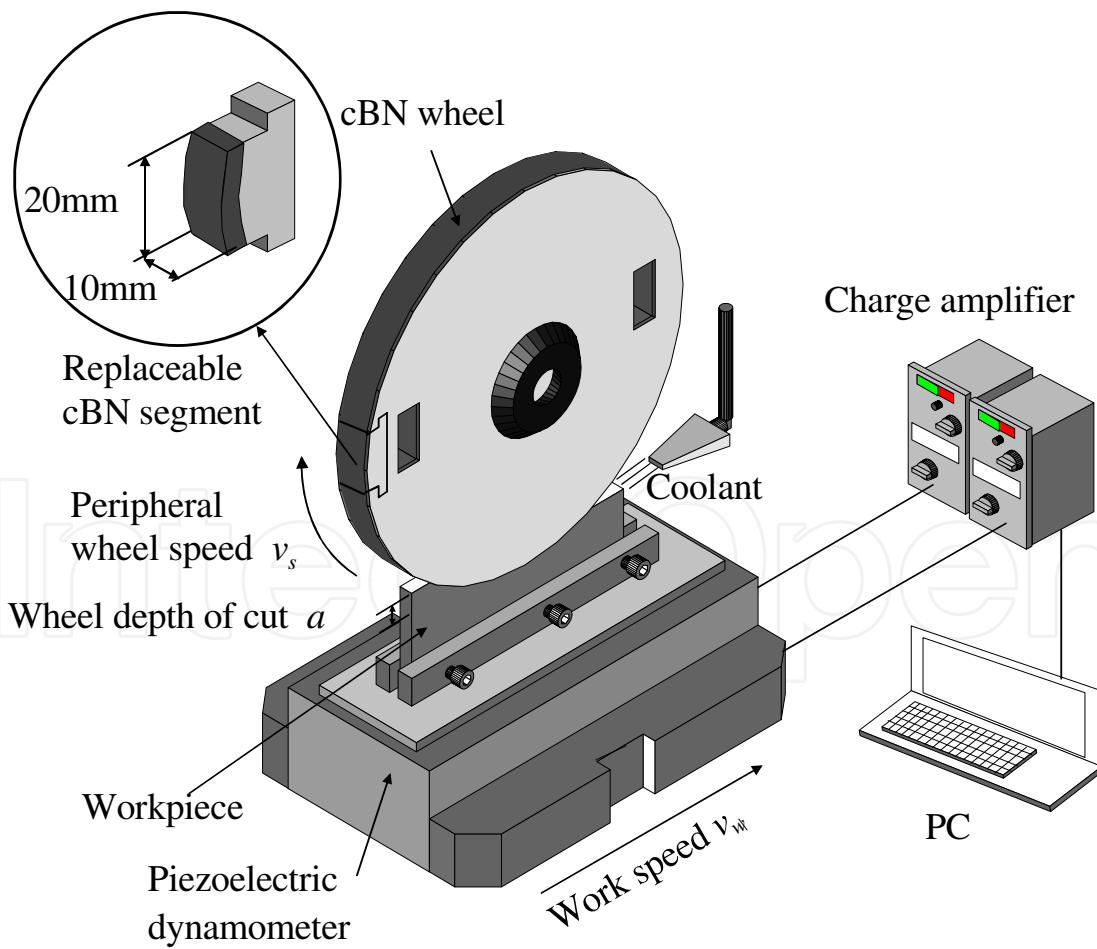


Fig. 3. Schematic illustration of the experimental setup.

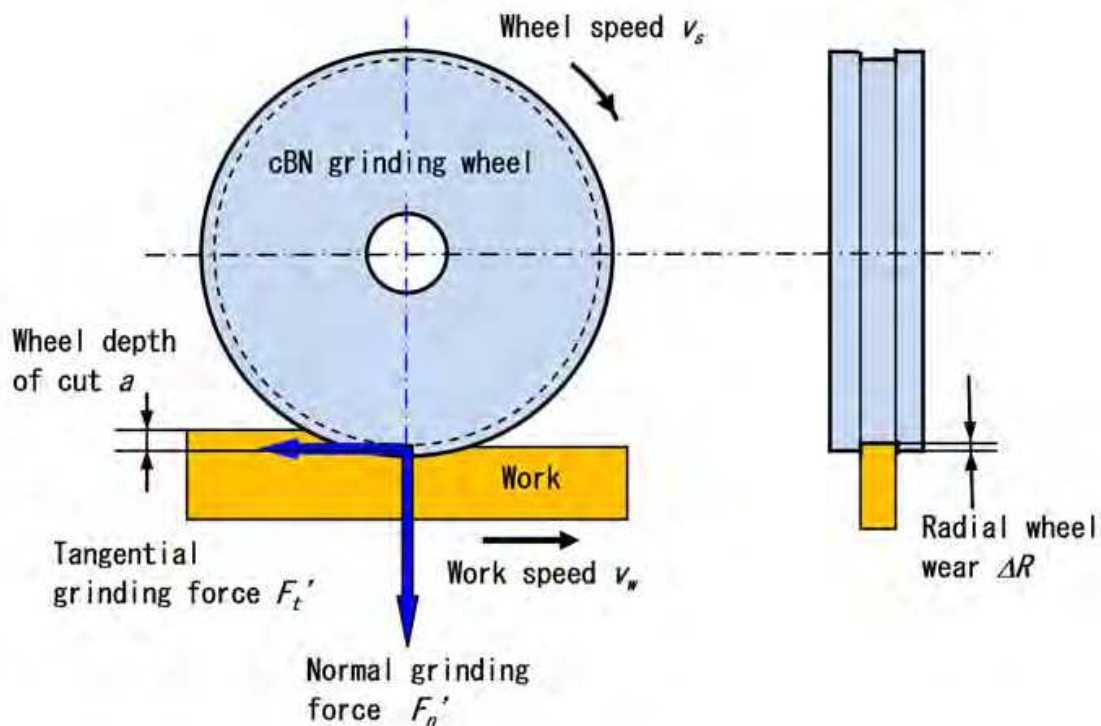


Fig. 4. Measurements of grinding characteristic parameters.

The experimental conditions are listed in Table 1. Representative single crystal cBN grain was used for cBN wheel. The dressing of cBN wheel was performed using a rotary diamond dresser (Dressing wheel: SD40Q75M) equipped with an AE sensor under the following dressing conditions: peripheral dressing speed 16.5 m/s, peripheral wheel speed ratio 0.5, dressing lead 0.1 mm/rev, dressing depth of cut  $2\mu\text{m}\times 5$  times. High speed steel SKH51/JIS (M2/ASTM) is used as the workpiece material.

Grinding method	Surface plunge grinding(Up-cut)
Grinding wheel	CBN80L100V Dimensions: $200^D\times 10^T$ [mm]
cBN grain	Single crystal cBN
Peripheral wheel speed $v_s$	33 [m/s]
Work speed $v_w$	0.1 [m/s]
Wheel depth of cut $a$	10 [ $\mu\text{m}$ ]
Grinding fluid	Soluble type (JIS W-2-2) 2% dilution
Workpiece	High speed steel (JIS/SKH51) Hardness: 65HRC Dimensions: $100^l\times 5^t\times 30^b$ [mm]

Table 1. Grinding conditions.

### 3.2 Measuring method of wheel surface profile with 3D-SEM

This 4-channel secondary electron (SE) detection system enables quantitative surface roughness measurements and enhances the topography by displaying the differential signal calculated from the 4 signals. The intensities of these detected signals are determined by the tilt angle of the specimen surface in relation to the geometric positioning of the detectors. The quantitative angular information can be obtained by the subtraction between the signal intensities of the detectors. By calculating 4 tilting angles (two in X-direction and two in Y-direction) on many spots in the X-Y matrix taken on the specimen, the surface topography of the specimen can be accurately re-constructed by integrating these angles over the matrix.

In this system, no eucentric tilting for stereo pairs is required, thereby simplifying operation and allowing much better precision and resolution than conventional SEMs using stereo photogrammetry. The vertical resolution in measuring a 3D profile using this 3D-SEM is 1 nm.

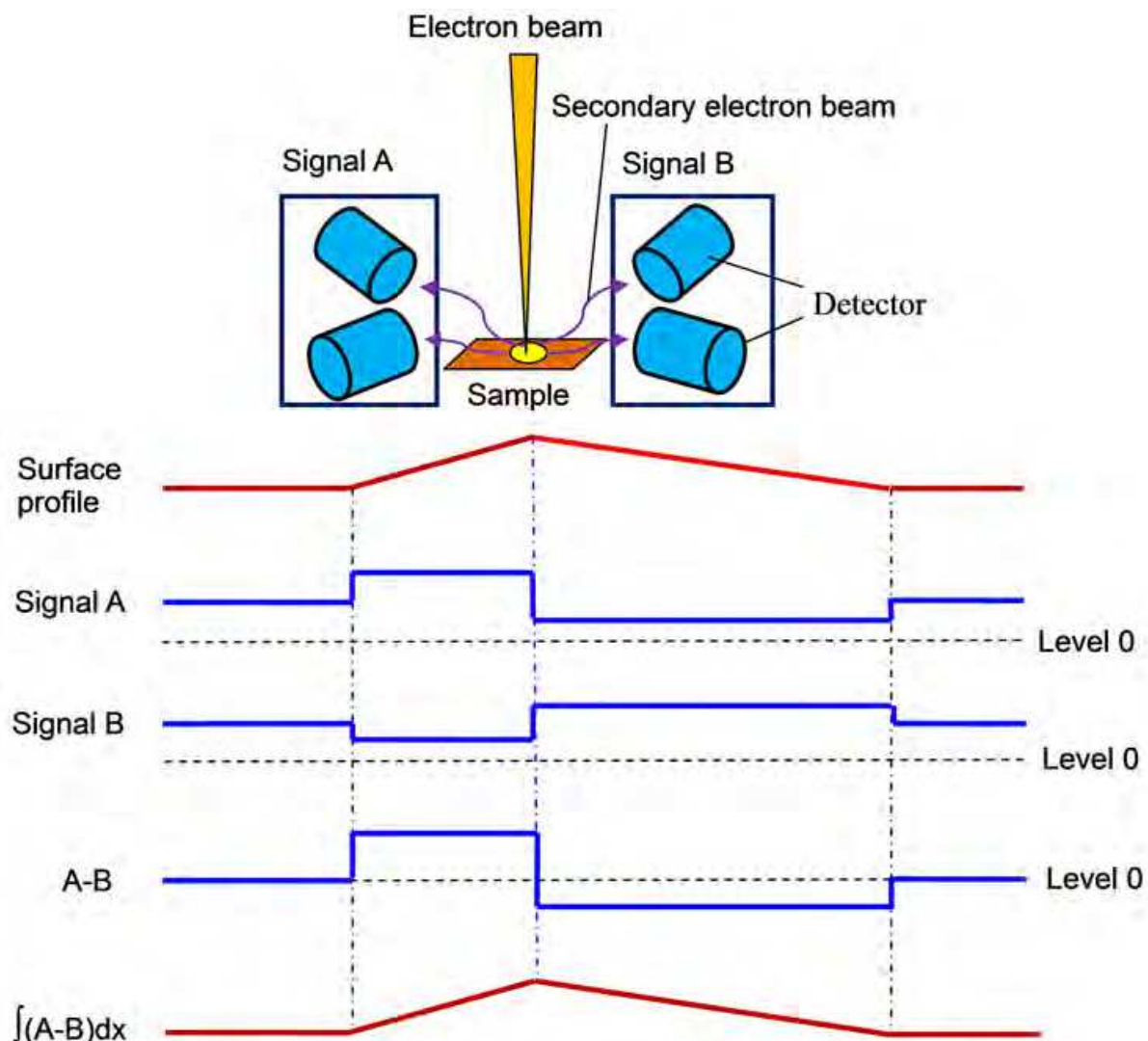


Fig. 5. Illustration of the 4-channel SE detector layout detailing the measurement principle of 3D-SEM.

#### 4. Grinding wheel wear and wheel working surface

Grinding wheel wear is an important consideration because adversely affects the shape and accuracy of ground surface. Grinding wheel wear by three different mechanisms: attritious grain wear, grain fracture and, and bond fracture, as shown in Fig.6. In attritious wear, the cutting edges of a sharp grain dull by attrition, developing a wear flat. Wear is caused by the interaction of the grain with the workpiece material, involving both physical and chemical reactions. These reactions are complex and involve diffusion, chemical degradation or decomposition of the grain, fracture at a microscopic scale, plastic deformation, and melting. If the wear flat caused by attritious wear is excessive, the grain becomes dull and grinding becomes inefficient and produces undesirable high temperatures. Optimally, the grain should fracture or fragment at a moderate rate, so that new sharp cutting edges are produced continuously during grinding. This phenomenon is self-sharpening. However, self-sharpening by a large fracture is not suitable for precision grinding, because it gives large wheel wear and bad surface roughness during grinding. Therefore, self-sharpening due to micro fracture as shown in Fig.6 is suitable for effective precision grinding, because it offers small wheel wear and good surface roughness. We call this phenomenon 'micro self sharpening'(Ichida, 2008).

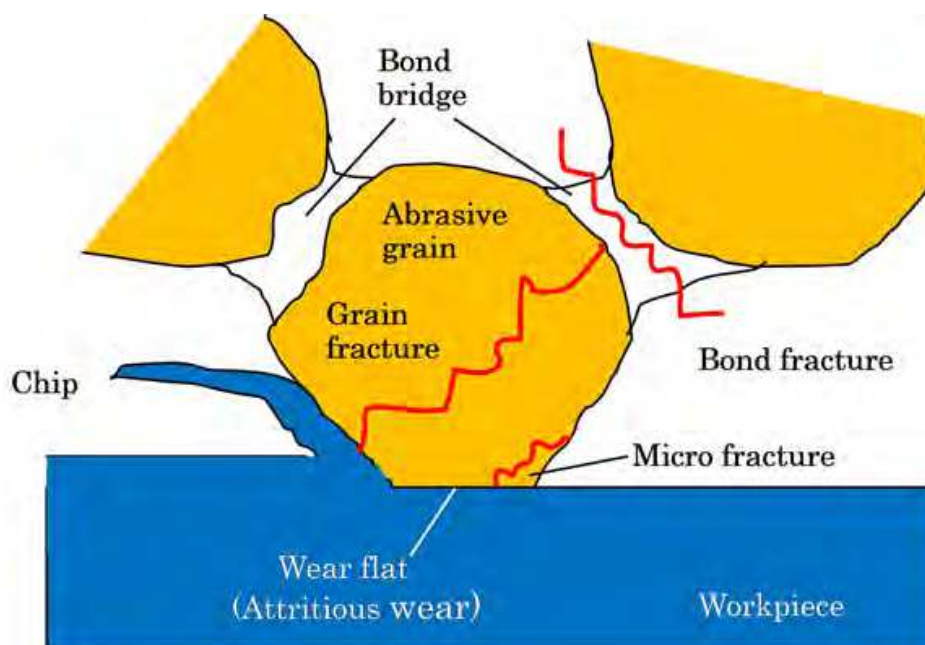


Fig. 6. Wear mechanisms of abrasive grain during grinding.

Fig. 7 shows the change in radial wheel wear  $\Delta R$  with increasing the accumulated stock removal (cumulative volume of material removed per unit grinding width)  $V_w'$  when grinding under the conditions indicated in Table 1. At the same time, some typical sequential SEM images of the wheel working surface with an increase of stock removal are shown in this figure. The wear process of grinding wheel can be divided into two different regions: a) initial wear region over stock removal range from 0 to 1000 mm<sup>3</sup>/mm, in which a rapid increase of wheel wear occurs with increasing stock removal, b) steady-state wear region over stock removal range larger than 1000 mm<sup>3</sup>/mm, in which the wheel wear rate maintains a nearly constant value. In the initial wear region, a releasing of grain due to bond fracture and grain

fracture are sometimes observed, as shown in grains C, D and so on. However, they are not observed so much in the steady-state wear region. The wheel wear in steady-state region dominantly occurs due to attritious wear and micro fracture, as shown in grains A, B and so on. As a typical example, a high magnification SEM image of grain A is shown in Fig.8 (a). Fig.8 (b) is its contour map. Wear flat developed due to attritious wear and some brittle surfaces generated by micro fracture can be observed on the point of the grain.

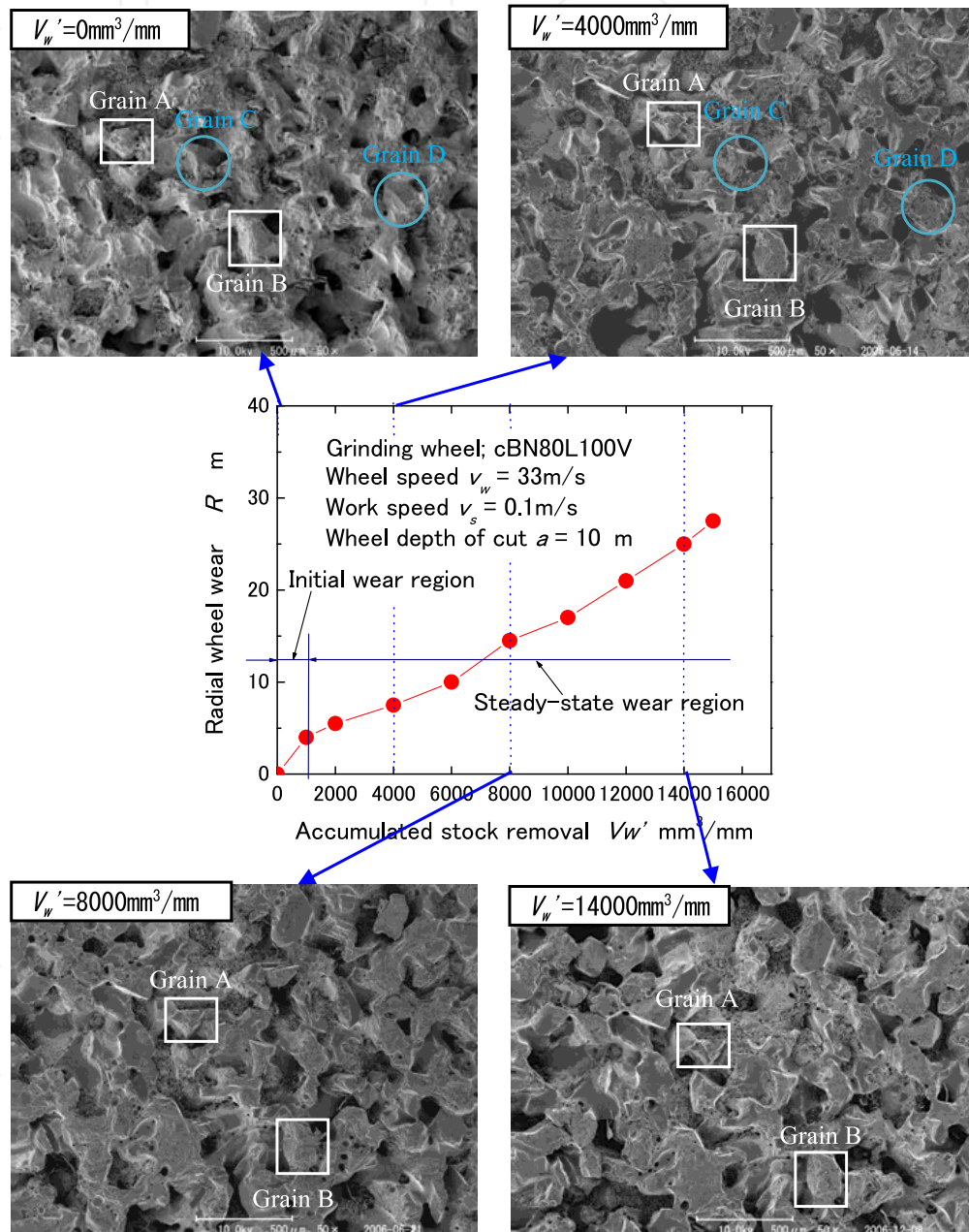


Fig. 7. Change of radial wheel wear with increasing stock removal and typical sequential SEM images of wheel working surface.

There is little research that has quantitatively evaluated self-sharpening phenomenon of grinding wheel. We have tried to grasp the actual behavior of self-sharpening and evaluate it by the attritious wear flat area percentage of the grain cutting edge (Ichida, 2008, 2009).

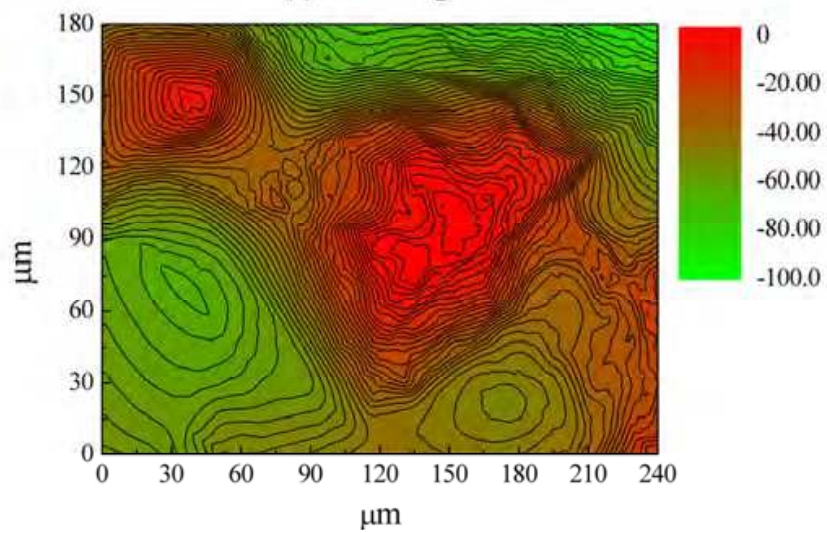
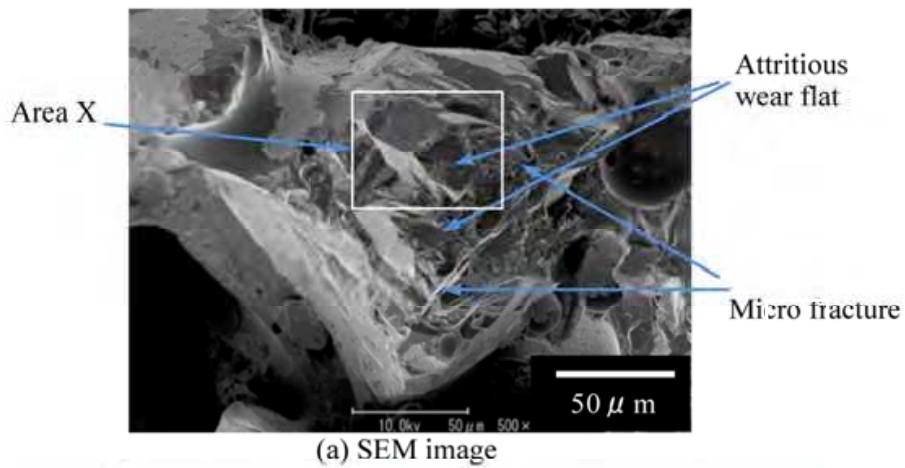


Fig. 8. High magnification SEM image and its contour map of grain A in Fig.7 ( $V_w=4\ 000\text{mm}^3/\text{mm}$ ).

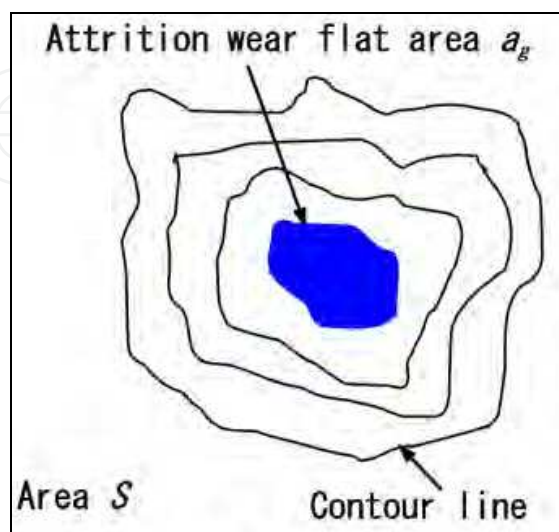


Fig. 9. Measuring method of attritious wear flat percentage.

Figure 9 shows the measuring method of the attritious wear flat percentage. Attritious wear flat area  $a_g$  in the area  $S$  to be observed is measured using SEM image and contour map made by 3D-profiles. Here, attritious wear flat percentage  $A_g$  is given by:

$$A_g = \frac{a_g}{S} \times 100[\%] \quad (6)$$

## 5. Self-sharpening phenomenon due to micro fracture of cutting edges

Grain cutting edges on the wheel surface change their shapes in various forms with the progress of wheel wear when the accumulated stock removal  $V_w'$  increases. Many sequential observations of the grain cutting edge with accumulated stock removal have been carried out using 3D-SEM. The typical result is shown in Fig. 10. Those are high magnification images of area X on grain A in Fig. 8(a).

The surface with a micro unevenness formed by the diamond dresser is observed on the tip of the grain cutting edge after dressing, as shown in Fig. 10 (a). And after grinding the stock removal  $V_w' = 500 \text{ mm}^3/\text{mm}$ , an attritious wear flat is observed in the center part on the top surface of the grain cutting edge, as shown in Fig. 10 (b). Moreover, at  $V_w' = 2000 \text{ mm}^3/\text{mm}$ , the wear flat becomes larger than that at  $V_w' = 500 \text{ mm}^3/\text{mm}$ , as indicated in the comparison between Figs. 10 (b) and (c). The ductile attritious wear flat area takes the largest value at  $V_w' = 2000 \text{ mm}^3/\text{mm}$  in the grinding process, as seen from all SEM images in Fig. 4. However, between the stock removals from 2000 to 4000  $\text{mm}^3/\text{mm}$ , some micro fractures take place at the lower left side part of cutting edge and consequently the wear flat area decreases a little, as indicated in the comparison between Figs. 10(c) and (d). Moreover, between the stock removals from 4000 to 10000  $\text{mm}^3/\text{mm}$ , as many micro fractures take place repeatedly, the ductile attritious wear flat area is decreased and some new sharp edges are formed on the top surface of cutting edge, as shown in the comparison between Figs. 10 (e) and (f).

In addition, between the stock removals from 10000 to 12000  $\text{mm}^3/\text{mm}$ , a small fracture takes place at the right side part of cutting edge and some new sharp edges are formed, and at the same time the wear flat is formed slightly in the center part on the cutting edge surface, as indicated in the comparison between Figs. 10 (f) and (g). Afterward, between the stock removals from 12000 to 14000  $\text{mm}^3/\text{mm}$ , some new sharp edges due to the micro fracture are observed in the middle part on the cutting edge top surface, while the new attritious wear flat is formed again at the upper part of the cutting edge, as indicated in the comparison between Figs. 10 (g) and (h).

Thus, although the grain cutting edges become dull due to the ductile attritious wear, they can reproduce and maintain their sharpness due to the micro fractures occurred repeatedly on their top surfaces. Namely, an actual behavior of the self-sharpening phenomenon due to the micro fracture may be grasped on the basis on the sequential SEM observation method used in this study.

## 6. Evaluation of self-sharpening using fractal dimension

As mentioned above, the shape of the cutting edges on the wheel working surface is variously changed due to the fracture wear or the attritious wear when the accumulated

stock removal increases. Such a complicated wear process is evaluated using 3D-fractal dimension. Fractal dimension is calculated in an area of  $27.4 \times 20.6 \mu\text{m}^2$  enclosed with white frame in Fig. 10. The center of these areas is almost located in the top part of the cutting edge that acts as an effective edge. The range of mesh size  $r$  is  $0.11 < r < 6.4 \mu\text{m}$ .

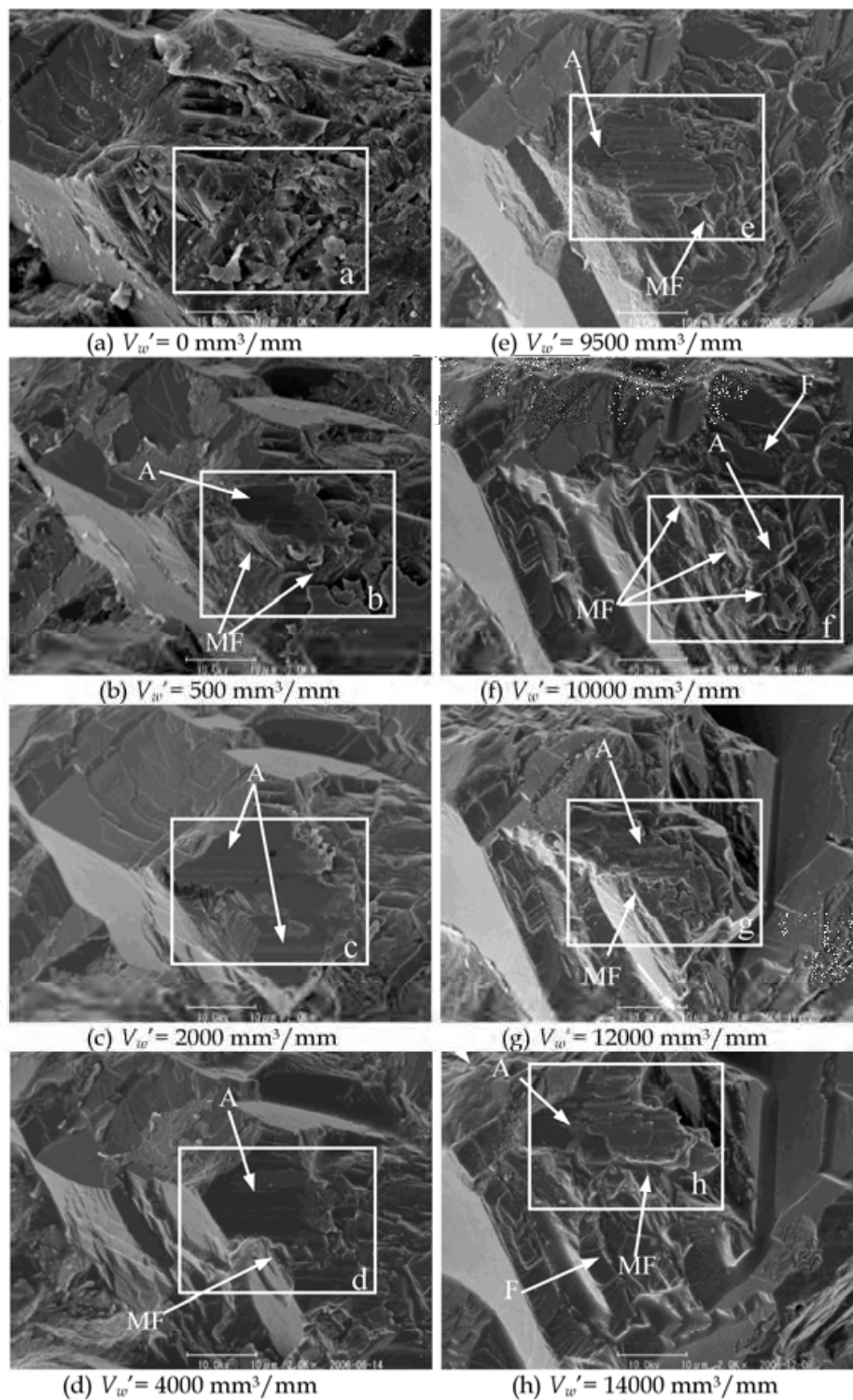


Fig. 10. Change in shape of grain cutting edge with accumulated stock removal (Area X on grain A in Fig.8(a)) (A: attritious wear, MF: micro fracture, F: fracture).

Figure 11 shows the 3D-profiles of the typical eight areas a, b, ..., h on the cutting edge used for fractal analysis (areas enclosed with white frame in Fig. 10). The relationships between mesh size  $r$  and surface area  $S(r)$  obtained in these typical eight areas are shown in Fig. 12. This figure indicates that the fractal nature is approved in a region of  $0.4 < r < 4 \mu\text{m}$ . Using this relationship, fractal dimension is calculated. The results obtained are shown in Fig. 13. The fractal dimension changes complexly and randomly when the accumulated stock removal increases.

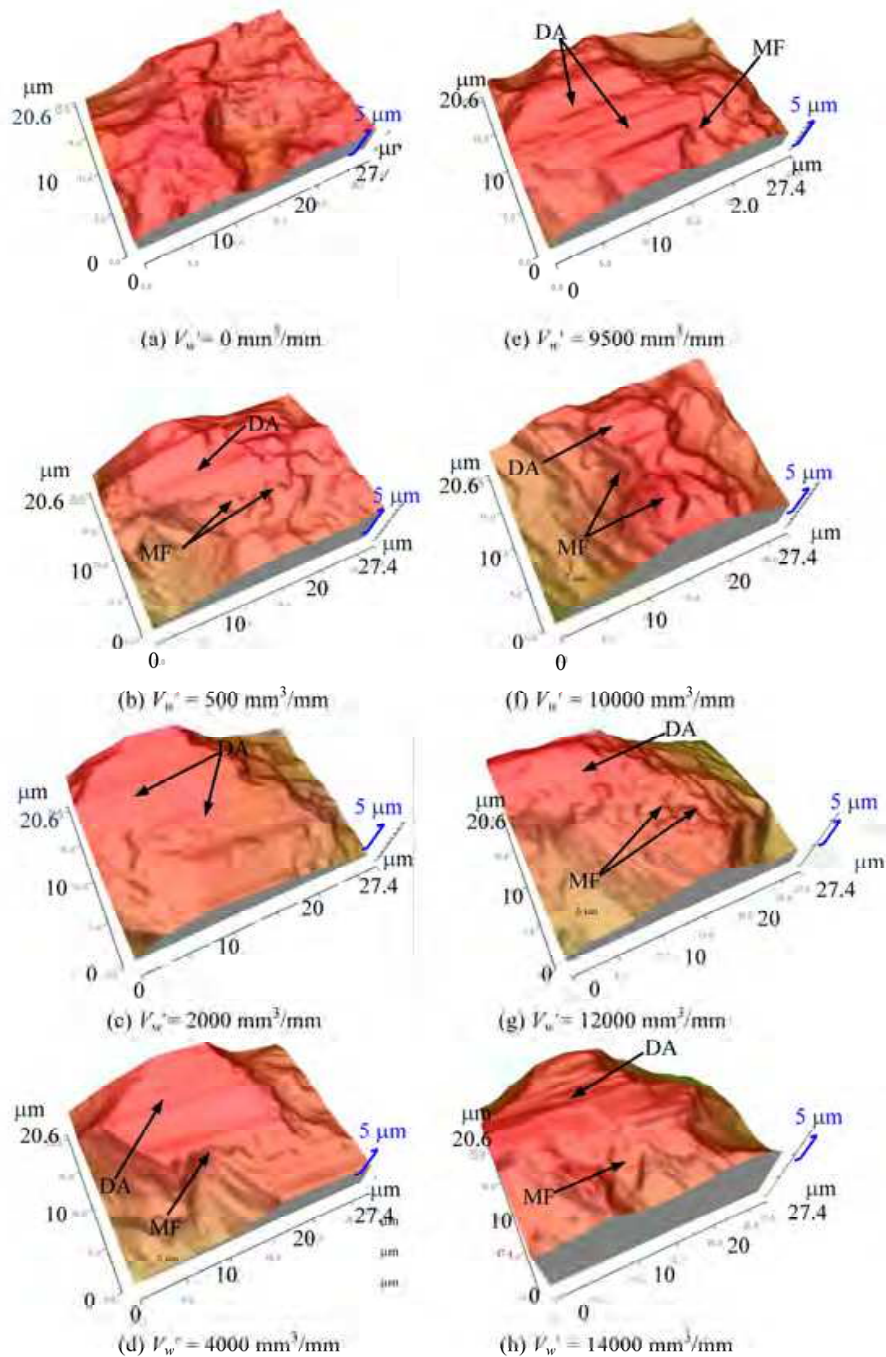


Fig. 11. Sequential 3D-profiles of typical area on grain cutting edge used for fractal analysis (DA: ductile attritious wear, MF: micro fracture).

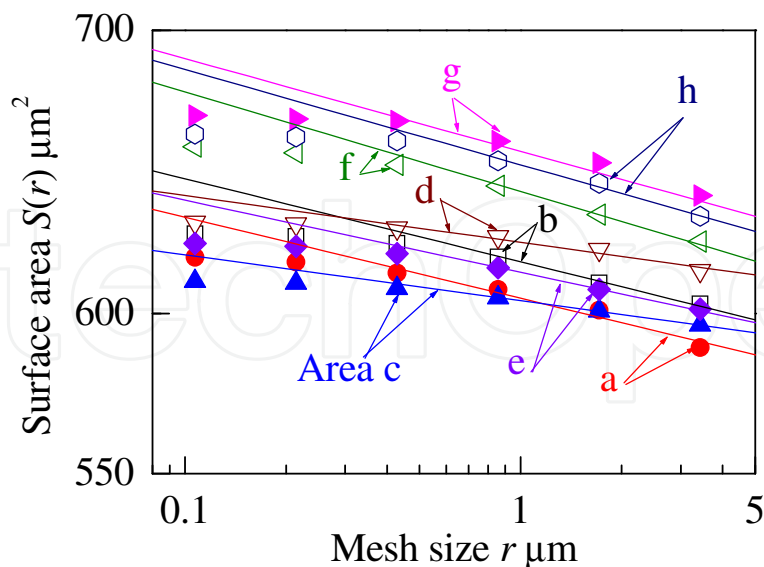


Fig. 12. Relationship between surface area  $S(r)$  and mesh size  $r$  in areas shown in Fig.11.

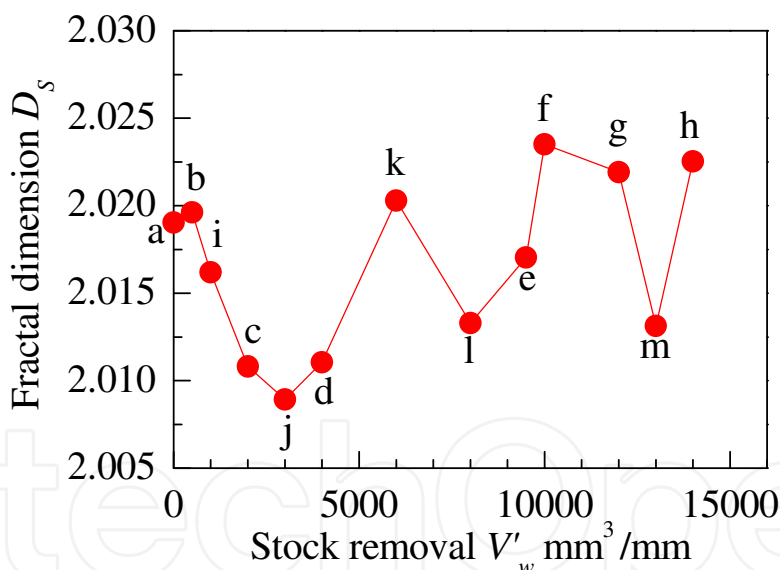


Fig. 13. Change in fractal dimension on top surface profile of grain cutting edge with accumulated stock removal.

To consider the reason for such complicated change of fractal dimension, the attritious wear flat area percentage of the cutting edge was measured. In this study, a percentage of ductile attritious wear area in same area of  $27.4 \times 20.6 \mu\text{m}^2$  used for fractal analysis is measured and defined as attritious wear flat area percentage  $A_g$ . Figure 14 shows the change in the attritious wear flat area percentage  $A_g$  of the grain cutting edge with increasing accumulated stock removal.

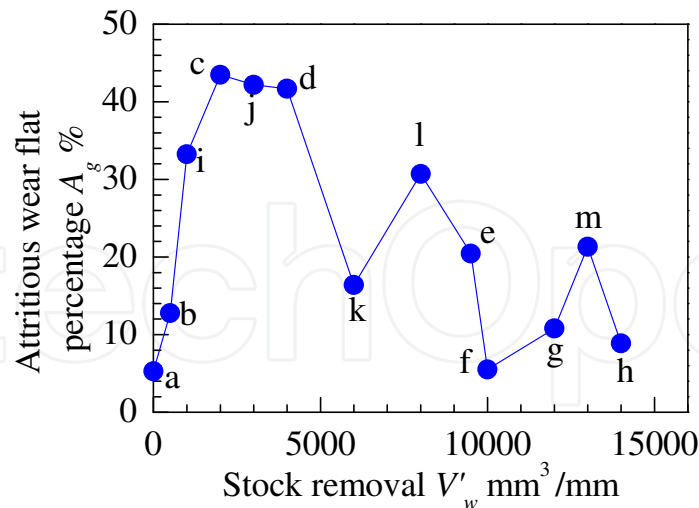


Fig. 14. Change in attritious wear flat percentage on top surface of grain cutting edge with accumulated stock removal.

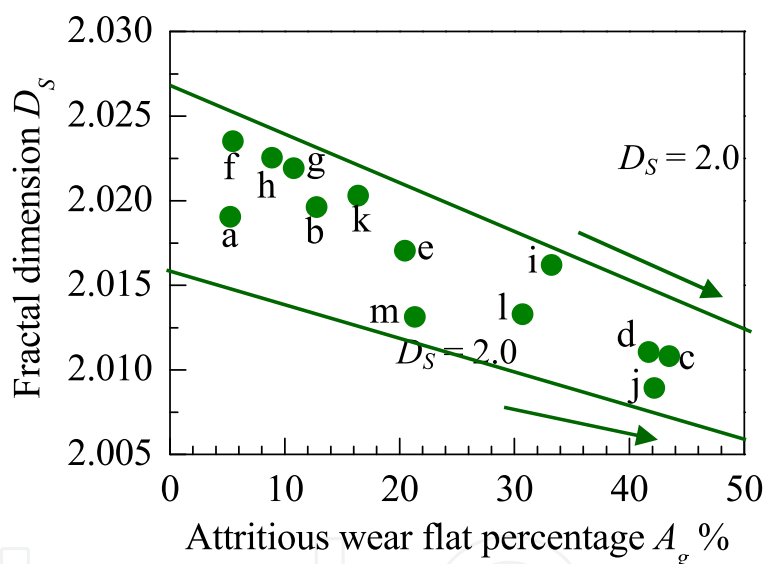


Fig. 15. Relationship between fractal dimension  $D_s$  and attritious wear flat percentage  $A_g$

As shown in Figs. 13 and 14, the cutting edge after dressing comparatively takes a high fractal dimension ( $D_s = 2.02$ ), because it has complicated surface with a micro ruggedness formed by the diamond dresser. And then, between the stock removals from 500 to 3000  $\text{mm}^3/\text{mm}$ , fractal dimension decreases because the attritious wear flat increases with the accumulated stock removal. In addition, between the stock removals from 2000 to 4000  $\text{mm}^3/\text{mm}$ , fractal dimension indicates the lowest value ( $D_s = 2.01$ ) because the attritious wear flat takes the highest value. Afterward, over a range of stock removals from 4000 to 6000  $\text{mm}^3/\text{mm}$ , fractal dimension tends to increase because the attritious wear flat decreases and new sharp cutting edges are formed by self-sharpening due to micro fractures. However, between the stock removals from 6000 to 8000  $\text{mm}^3/\text{mm}$ , fractal dimension decreases slightly because of a little increase in attritious wear flat area. Moreover, fractal dimension increases rapidly over a range of stock removals from 8000 to 10000  $\text{mm}^3/\text{mm}$

because the attritious wear flat area decreases and micro fracture occurs repeatedly, i.e., self-sharpening due to micro fracture takes place actively. Afterward, although the fractal dimension decreases because of increasing in attritious wear flat at the stock removal 13000 mm<sup>3</sup>/mm, it increases again because self-sharpening due to micro fracture takes place actively over a range of stock removals from 13000 to 14000 mm<sup>3</sup>/mm.

As mentioned above, self-sharpening of the grain cutting edge can be characterized using fractal dimension. Especially, these results show that there is a close relationship between fractal dimension  $D_s$  and attritious wear flat percentage  $A_g$ . Figure 15 shows relationship between fractal dimension and attritious wear flat percentage. The alphabets in Fig.15 correspond to those in Figs.10, 11, 12, 13 and 14. As shown in this figure, fractal dimension decreases with increasing the attritious wear flat percentage and then becomes 2.0 at  $A_g = 100\%$  (perfect smooth surface) as a limit value. Thus, there is a negative correlation between fractal dimension and attritious wear flat percentage.

## 7. Effect of self-sharpening on grinding characteristics

Fig.16 and 17 show the changes of grinding forces and ground surface roughness with increasing accumulated stock removal, respectively. Under this grinding condition, grinding forces maintains a stable level in the steady-state wear region. Especially, tangential grinding force keeps a small variation between 4 and 6 N/mm in this wear region. On the other hand, although surface roughness increases with increasing stock removal, its increasing rate maintains comparatively low level. Thus, high grinding ability of cBN wheel is brought from such self-sharpening due to micro fracture of grain cutting edges, that is, micro self-sharpening phenomenon.

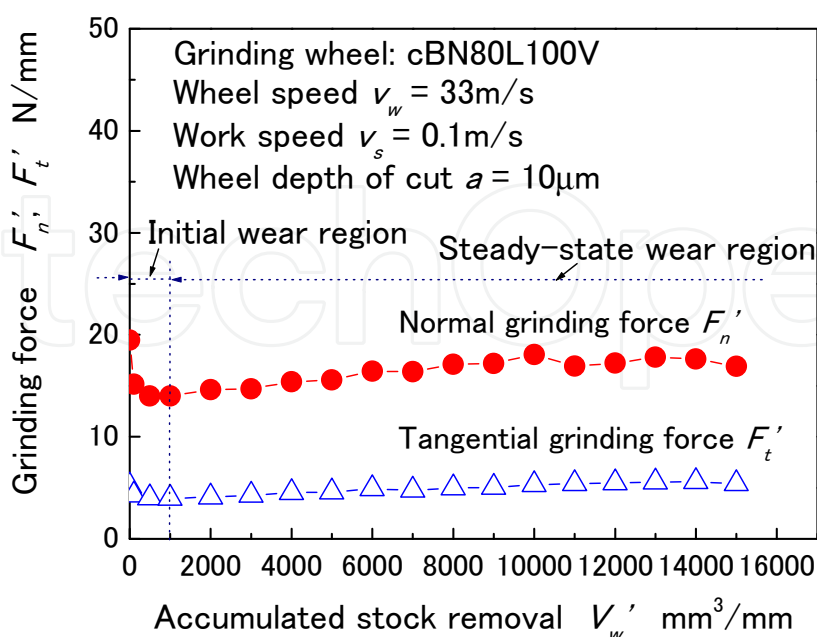


Fig. 16. Changes in grinding forces with increasing accumulated stock removal.

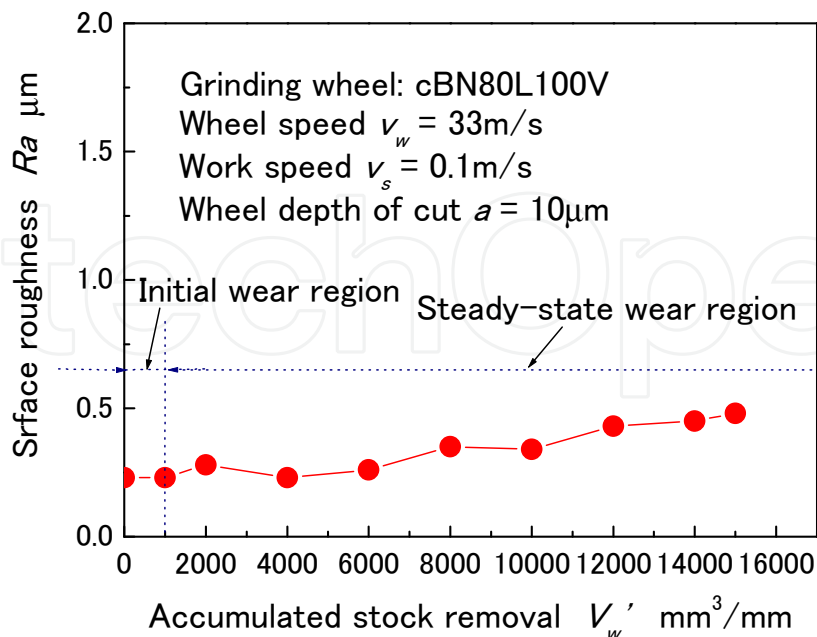


Fig. 17. Change of ground surface roughness with increasing accumulated stock removal.

## 8. Conclusions

The changes in three-dimensional surface profile of grain cutting edge in the grinding process with cBN wheels have been measured using a 3D-SEM and evaluated by means of fractal dimension. The main results obtained in this study are summarized as follows;

1. Actual behavior of self-sharpening phenomenon due to the micro fracture in the grinding process can be grasped using sequential observation method with 3D-SEM.
2. The fractal dimension for surface profile of the cutting edge formed by the micro fracture is higher than that of the cutting edge formed due to ductile attritious wear. An increase in ductile attritious wear flat area on the grain cutting edge results in a decrease in fractal dimension for its surface profile.
3. The complicated changes in shape of the cutting edge due to self-sharpening can be evaluated quantitatively using fractal dimension.

## 9. Acknowledgment

This research was supported in part by Grants-in-Aid for General Science Research (C) (No.19560106) from the Ministry of Education, Culture, Sports, Science and Technology of Japan.

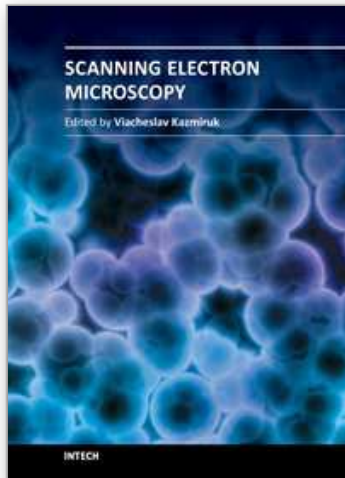
## 10. References

- Yoshikawa, H. (1960). Process of Wear in Grinding Wheel with Fracture of Bond and Grain, *Journal of the Japan Society for Precision Engineering*, Vol.26, No. 11, (1960), pp.691-700, ISSN0912-0289

- Tsuwa, H. (1961). On the Behaviors of Abrasive Grains in Grinding Process (Part 4)- Microscopic Observations of Cutting Edges-, *Journal of the Japan Society for Precision Engineering*, Vol. 27, No. 11,(1961), pp. 719-725 , ISSN0912-0289
- Kalpakjian, S. (1995), *Manufacturing Engineering and Technology*, Third Edition, Addison-Wesley Publishing Company Inc. , ISBN 0-201-53846-6, New York, pp.795-798.
- Show, M. C. (1996), *Principles of Abrasive Processing*, Clarendon Press, Oxford, ISBN 0-19-859021-0, pp.55-62.
- Malkin, S. (1989). *Grinding Technology: Theory and Applications of Machining with Abrasives*, Ellis Horwood Limited, Chichester, UK, PP.197-202. ISBN 0-85312-756-5
- Ichida, Y.; Fredj, N. B. & Usui, N. (1995). The Micro Fracture Wear of Cutting Edges in CBN Grinding, *The Second International ABTEC Conference*, Vol. 11, (1995), pp. 501-504.
- Ichida, Y.; Kishi, K.; Suyama, Y. & Okubo, J. (1989). Study of Creep Feed Grinding with CBN Wheels, -Characteristics of Wheel Wear-, Vol.55, No.8, pp.1468-1474, ISSN0912-0289
- Ichida, Y. & Kishi, K. (1997). The Development of Nanocrystalline cBN for Enhanced Superalloy Grinding Performance, *Transactions of the ASME, Journal of Manufacturing, Science and Engineering*, Vol. 119, No. 1, (1997), pp.110-117. ISSN 1087-1357
- Webster, J. & Tricard, M. (2004). Innovations in Abrasive Production for Precision Grinding, *Annals of the CIRP*, Vol.53, No.2, pp.597-617, ISSN 0007-8506
- Ichida, Y.; Sato, R.; Morimoto, Y. & Inoue, Y. (2006). Profile Grinding of Superalloys with Ultrafine-Crystalline cBN Wheels, *JSME International Journal, Series C*, Vol.49, No.1, pp.94-99, ISSN 1344-7653.
- Guo, C.; Shi, Z.; Attia, H. & McIntosh, D. (2007). Power and Wheel Wear for Grinding Nickel Alloy with Plated CBN Wheels, *Annals of the CIRP*, Vol.56, No.1, pp.343-346, ISSN 0007-8506
- Comley, P.; Walton, I.; Jin, T. & Stephenson, D. J. (2006). A High Material Removal Rate Grinding Process for the Production of Automotive Crankshafts, *Annals of the CIRP*, Vol.55, No.1, pp.347-350, ISSN 0007-8506
- Mandelbrot, B. B. (1983). *The Fractal Geometry of Nature*, Freeman, W. H. and Company, New York, (1983), pp.109-111, ISBN4-532-06254-3
- Mandelbrot, B. B.; Passoja, D. E. & Paullay, A. J. (1984). Fractal Characterization of Fracture Surfaces of Metals, *Nature*, Vol. 308, pp.1571-1572, ISSN 0028-0836.
- Hagiwara, S.; Obikawa, T. & Yanai, H. (1995). Evaluation of Lapping Grains Based on Shape Characteristics, *Journal of the Japan Society for Precision Engineering*, Vol. 61, No.12, pp.1760-1764, ISSN0912-0289
- Itoh, N.; Tsukada, T.& Sasajima, K. (1990). Three-Dimensional Characerization of Engineering Surface by Fractal Dimension, *Bulletin of the Japan Society for Precision Engineering*, Vol.24, No.2, pp.148-149.
- Sakai, T.; Sakai, T. & Ueno, A. (1998). Fractal Analysis of Metal Surface Mechanically Finished by Several Methods, *Transactions of the Japan Society of Mechanical Engineers, Series A*, Vol. 64, No. 620, (1998-4), pp.1104-1112, ISSN 1884-8338.
- Fujimoto, M.; Ichida, Y.; Sato, R. & Morimoto, Y. (2006), Characterization of Wheel Surface Topography in cBN Grinding, *JSME International Journal, Series C*, Vol.49, No.1, pp.106-113, ISSN 1344-7653.

- Ichida, Y.; Sato, R.; Fujimoto, M. & Tanaka, H. (2008), Fractal Analysis of Grain Cutting Edge Wear in Superabrasive Grinding, *JSME Journal of Advanced Mechanical Design, Systems, and Manufacturing*, Vol.2, No.4, pp.640-650 ISSN 1881-3054 .
- Ichida, Y.; Sato, R.; Fujimoto, M. & Fredj, N. B. (2009). Fractal Analysis of Self-Sharpening Phenomenon in cBN Grinding, *Key Engineering*, Vols. 389-390, (2009), pp.42-47, ISBN-13978-0-87849-364-7
- Ichida, Y.; Fujimoto, M.; Akbari, J. & Sato, R. (2008). Evaluation of Cutting Edge wear in cBN Grinding Based on Fractal Analysis, *6th International Scientific and technical Symposium on Manufacturing and Materials*, Monastir, Tunisia, pp.287-294.

IntechOpen



## **Scanning Electron Microscopy**

Edited by Dr. Viacheslav Kazmiruk

ISBN 978-953-51-0092-8

Hard cover, 830 pages

**Publisher** InTech

**Published online** 09, March, 2012

**Published in print edition** March, 2012

Today, an individual would be hard-pressed to find any science field that does not employ methods and instruments based on the use of fine focused electron and ion beams. Well instrumented and supplemented with advanced methods and techniques, SEMs provide possibilities not only of surface imaging but quantitative measurement of object topologies, local electrophysical characteristics of semiconductor structures and performing elemental analysis. Moreover, a fine focused e-beam is widely used for the creation of micro and nanostructures. The book's approach covers both theoretical and practical issues related to scanning electron microscopy. The book has 41 chapters, divided into six sections: Instrumentation, Methodology, Biology, Medicine, Material Science, Nanostructured Materials for Electronic Industry, Thin Films, Membranes, Ceramic, Geoscience, and Mineralogy. Each chapter, written by different authors, is a complete work which presupposes that readers have some background knowledge on the subject.

### **How to reference**

In order to correctly reference this scholarly work, feel free to copy and paste the following:

Yoshio Ichida (2012). Fractal Analysis of Micro Self-Sharpening Phenomenon in Grinding with Cubic Boron Nitride (cBN) Wheels, Scanning Electron Microscopy, Dr. Viacheslav Kazmiruk (Ed.), ISBN: 978-953-51-0092-8, InTech, Available from: <http://www.intechopen.com/books/scanning-electron-microscopy/fractal-analysis-of-self-sharpening-phenomenon-in-grinding-with-cubic-boron-nitride-cbn-wheel>

**INTECH**  
open science | open minds

### **InTech Europe**

University Campus STeP Ri  
Slavka Krautzeka 83/A  
51000 Rijeka, Croatia  
Phone: +385 (51) 770 447  
Fax: +385 (51) 686 166  
[www.intechopen.com](http://www.intechopen.com)

### **InTech China**

Unit 405, Office Block, Hotel Equatorial Shanghai  
No.65, Yan An Road (West), Shanghai, 200040, China  
中国上海市延安西路65号上海国际贵都大饭店办公楼405单元  
Phone: +86-21-62489820  
Fax: +86-21-62489821

© 2012 The Author(s). Licensee IntechOpen. This is an open access article distributed under the terms of the [Creative Commons Attribution 3.0 License](#), which permits unrestricted use, distribution, and reproduction in any medium, provided the original work is properly cited.

IntechOpen

IntechOpen